 doi:10.20944/preprints202208.0217.v1

Article

Ferromagnetic coupling and single-ion magnet phenomenon in mononuclear ruthenium(III) complexes based on guanine nucleobase

Marta Orts-Arroyo,[1] Nicolás Moliner,[1] Francesc Lloret[1] and José Martínez-Lillo[1,*]

[1]Instituto de Ciencia Molecular (ICMol)/Departament de Química Inorgànica, Universitat de València, c/Catedrático José Beltrán 2, Paterna, 46980, València, Spain; marta.orts-arroyo@uv.es (M.O.-A.); fernando.moliner@uv.es (N.M.); francisco.lloret@uv.es (F.L.)

* Correspondence: f.jose.martinez@uv.es; Tel.: +34-9635-44460

Abstract: Two mononuclear Ru^{III} complexes of formula *trans*-[$RuCl_4$(Hgua)(dmso)]·$2H_2O$ (**1**) and *trans*-[$RuCl_4$(Hgua)(gua)]·$3H_2O$ (**2**) [Hgua = protonated guanine (gua), dmso = dimethyl sulfoxide] have been synthesized and characterized magnetostructurally. **1** and **2** crystallize in the monoclinic system with space groups $P2_1/n$ and Pc, respectively. Each Ru^{III} ion in **1** and **2** is bonded to four chloride ions and one (**1**) or two (**2**) nitrogen atoms from guanine molecules and one sulfur atom (**1**) of a dmso solvent molecule, generating quasi regular octahedral geometries in both cases. In their crystal packing, the Ru^{III} complexes are connected through an extended network of N-H···Cl hydrogen bonds and π···Cl intermolecular interactions, forming novel supramolecular structures of this paramagnetic 4d ion. Variable-temperature dc magnetic susceptibility data were obtained from polycrystalline samples of **1** and **2** and their plots show a different magnetic behavior. While **1** is a ferromagnetic compound at low temperature, **2** exhibits a behavior of magnetically isolated mononuclear Ru^{III} complexes with S = 1/2. The study on ac magnetic susceptibility data reveal slow relaxation of the magnetization, when external dc fields are applied, only for **2**. These results highlight the presence of field-induced single-ion magnet (SIM) behavior for this mononuclear guanine-based Ru^{III} complex.

Keywords: Ruthenium; crystal structures; ferromagnetic coupling; molecular magnetism; single-ion magnet.

1. Introduction

Heteroleptic mononuclear Ru(III) complexes are especially relevant for the study of molecular systems with very appealing biological and biochemical properties [1]. The most successful examples of Ru(III) complexes are prepared with imidazole and indazole ligands, namely the anionic complexes *trans*-[tetrachloro(dimethyl sulfoxide)(imidazole)ruthenate(III)] (NAMI-A) and *trans*-[tetrachlorobis(indazole)ruthenate(III)] (KP1019), which are effective anticancer and antimetastatic compounds that have been investigated in clinical trials [2-3]. Most metal-based anti-tumor compounds interact strongly with DNA, however, NAMI-A acts as an inhibitor of the metastatic potential of tumor and its activity is not related with DNA binding in cancer cells [4].

Similar studies have been performed on ruthenium complexes based on nitrogenous bases [5-8]. In 2004, the first guanine-based Ru(III) compound of formula *trans*-[$RuCl_4$(Hgua)(dmso)]·$2H_2O$ (Hgua = monoprotonated guanine) was investigated [5]. It was prepared by refluxing a mixture of *trans*-[$RuCl_4(dmso)_2$]$^-$ complex and acyclovir in ethanol and HCl. It was characterized by single-crystal X-ray diffraction and the *in vitro* antitumor activity was also evaluated [5], but the study of its magnetic properties, as for the most of these mononuclear Ru^{III} complexes, remain largely unexplored. Indeed, in

Preprints (www.preprints.org) | NOT PEER-REVIEWED | Posted: 11 August 2022 doi:10.20944/preprints202208.0217.v1

the literature there exists only one mononuclear Ru^{III} complex exhibiting Single-Ion Magnet (SIM) behavior reported up to date, the Ru^{III} system of formula $[RuCl_3(PPh_3)_2(MeCN)]$ (PPh_3 = triphenylphosphine) [9].

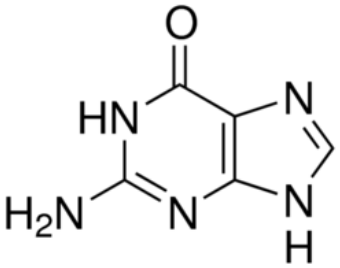

Scheme 1. Molecular structure of guanine.

In this work, we report the synthesis, crystal structure and the study of the magnetic properties of two Ru^{III} complexes of formula *trans*-$[RuCl_4(Hgua)(dmso)]\cdot 2H_2O$ (**1**) and *trans*-$[RuCl_4(Hgua)(gua)]\cdot 3H_2O$ (**2**) [Hgua = protonated guanine (gua), dmso = dimethyl sulfoxide], which are based on the guanine ligand (Scheme 1). While **1** is a novel ferro-magnetic complex, **2** is the second reported example of SIM based on Ru^{III} metal ion.

2. Results and Discussion

2.1 Description of the Crystal Structures

The crystal structure of compound **1** was previously reported elsewhere, and was deposited with identifier ARAMUB [5]. Nevertheless, we include here some structural data and details, which are useful to discuss and understand its magnetic properties (Table 1). Compounds **1** and **2** crystallize in monoclinic space groups ($P2_1/n$ and Pc for **1** and **2**, respectively). The crystal structure of **1** is made up of neutral $[RuCl_4(Hgua)(dmso)]$ units, whereas that of **2** is made up of neutral $[RuCl_4(Hgua)(gua)]$ units. In both crystal structures, hydration H_2O molecules are also present (Figure 1).

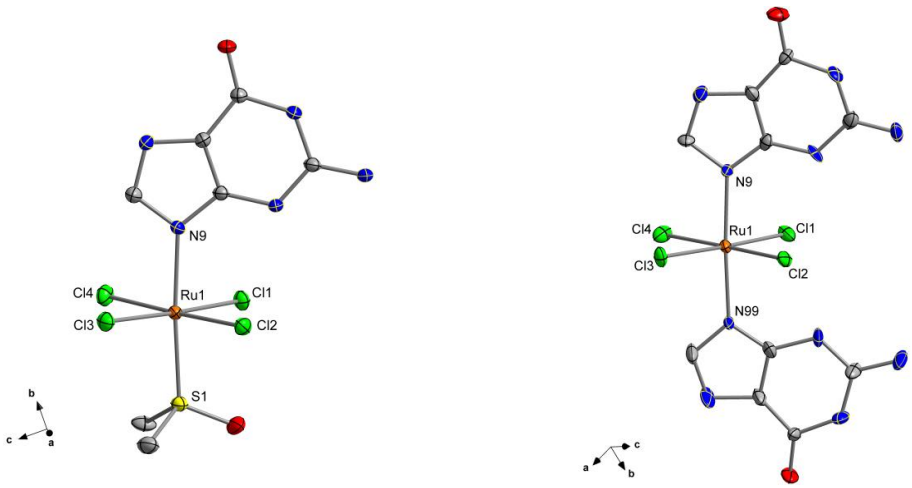

(**a**) (**b**)

Figure 1. View of the $[RuCl_4(Hgua)(dmso)]$ and $[RuCl_4(Hgua)(gua)]$ complexes showing the atom numbering of the Ru(III) metal ions together with those of their chromophores in **1** (**a**) and **2** (**b**). Water molecules and H atoms have been omitted for clarity. Thermal ellipsoids are shown at the 50% of probability.

In **1**, the Ru(III) ion is six-coordinate and bonded to four chloride ions, one sulfur atom from a dimethyl sulfoxide molecule and one nitrogen atom from one protonated guanine molecule. In **2**, the Ru(III) ion is bonded to four chloride ions and two nitrogen

Preprints (www.preprints.org) | NOT PEER-REVIEWED | Posted: 11 August 2022 doi:10.20944/preprints202208.0217.v1

atoms from two guanine ligands (Figure 1). The average values of the Ru-Cl bond lengths are 2.353(1) and 2.350(1) Å for **1** and **2**, respectively. The Ru-N bond length in **1** [2.107(4) Å] is somewhat longer than the average value of the Ru-N bond lengths in **2** [2.081(1) Å]. In both cases, the central metal ion exhibits two axial bonds [Ru-S (**1**) and Ru-N (**1** and **2**)] which are shorter than those of the equatorial bonds [Ru-Cl (**1** and **2**)], generating *quasi* regular octahedral geometries. In **2**, the two guanine molecules are pretty much planar and form an intramolecular angle between them of approximately 2.0(1)°. In **1** and **2**, the C-C, C-N and C-O bond lengths of the guanine ligands are as previously reported for this molecule when coordinated through N9 to 4d/5d metal centers [10-13].

Table 1. Crystal data along with structure refinement values for compounds **1** and **2**.

Compound	**1**	**2**
Formula	$C_7H_{16}N_5O_4SCl_4Ru$	$C_{10}H_{11}N_{10}O_5Cl_4Ru$
M_r/g mol^{-1}	509.18	594.16
Crystal system	monoclinic	monoclinic
Space group	$P2_1/n$	Pc
a/Å	9.836(1)	7.319(1)
b/Å	13.326(1)	11.433(1)
c/Å	12.886(1)	11.402(1)
α/°	90(1)	90(1)
β/°	93.04(1)	91.64(1)
γ/°	90(1)	90(1)
V / Å^3	1686.6(1)	953.7(1)
Z	4	2
D_c/g cm^{-3}	2.005	2.069
μ(Mo-K$_\alpha$)/mm^{-1}	1.708	1.433
F(000)	1012	586
Goodness-of-fit on F^2	1.435	1.073
R_1 [$I > 2\sigma(I)$]	0.0340	0.0591
wR_2 [$I > 2\sigma(I)$]	0.0350	0.1552

In the crystal lattice of compound **1**, adjacent [$RuCl_4$(Hgua)(dmso)] units are connected through H-bonding interactions between carbonyl and amino groups of protonated guanine and dmso ligands, which generate one-dimensional motifs growing offshore the *b* crystallographic axis [O···N distances covering the range *ca.* 2.72(1)-2.81(1) Å; (a) = -x+3/2, y+1/2, -z+5/2]. These chains are also linked through additional H bonds involving water molecules and forming a 2D framework (Figure 2) [Ow···N and Ow···Cl distances of *ca.* 2.734(1) and 3.367(1) Å, respectively; (b) = x+3/2, y+1/2, -z+3/2]. In **1**, Cl···π contacts covering the range 3.24(1)-3.53(1) Å occur and lead to the formation of Ru-Cl···π···Cl-Ru interactions between neighboring [$RuCl_4$(Hgua)(dmso)] units (Figure 2), this being a motif which have been observed previously in systems displaying intermolecular ferromagnetic coupling [14,15].

Preprints (www.preprints.org) | NOT PEER-REVIEWED | Posted: 11 August 2022 doi:10.20944/preprints202208.0217.v1

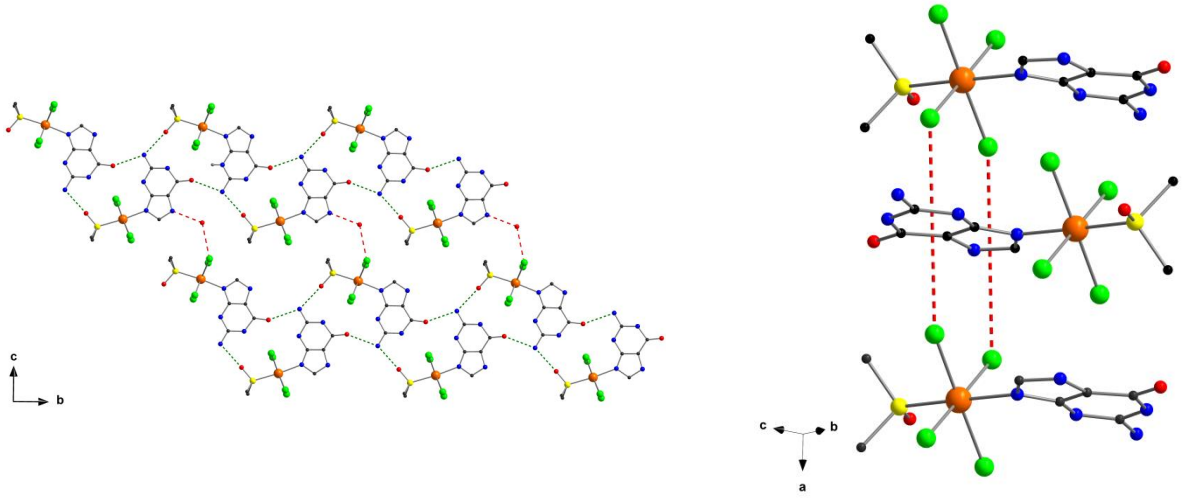

(**a**) (**b**)

Figure 2. (**a**) A fragment of the crystal of **1** showing hydrogen bonds involving [$RuCl_4$(Hgua)(dmso)] units (dashed green lines), and [$RuCl_4$(Hgua)(dmso)] complexes and water molecules (dashed red lines), along the crystallographic *a* axis; (**b**) Detail of the Ru–Cl···π···Cl–Ru interaction (dashed red lines) generated by alternate [$RuCl_4$(Hgua)(dmso)] complexes in **1**.

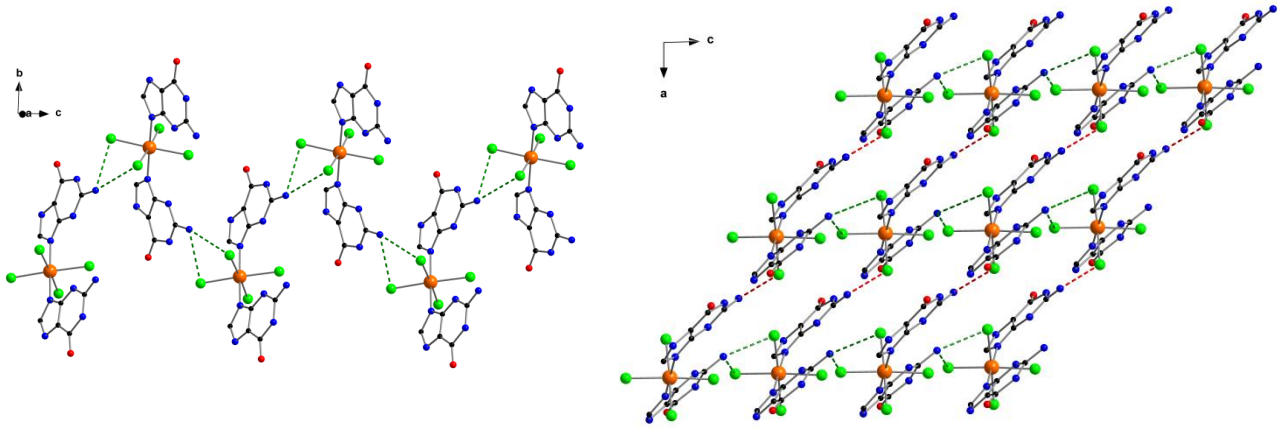

(**a**) (**b**)

Figure 3. (**a**) Detail of the zig-zag chain formed through bifurcated three-centered hydrogen bonds (dashed green lines) between mononuclear [$RuCl_4$(Hgua)(gua)] units in **2**; (**b**) 2D arrangement of [$RuCl_4$(Hgua)(gua)] complexes in **2** connected through additional hydrogen bonds (dashed red lines) and viewed along the crystallographic *b* axis.

In the crystal packing of **2**, N–H···$(Cl)_2$ type hydrogen bonds between amino groups and chloride ions of adjacent [$RuCl_4$(Hgua)(gua)] units form zig-zag 1D motifs, that grow along the crystallographic *c* axis [Cl1···N22a distance = 3.273 Å and Cl4b···N22 distance = 3.285 Å; being (a) = x, -y+2, z-1/2 and (b) = x, -y+2, z+1/2, respectively] (Figure 3). Longer H-bonded N–H···Cl interactions of *ca.* 3.377 Å connect these chains forming a 2D framework [Cl3···N2c distance = 3.377 Å; (c) = x+1, -y+1, z-1/2] in **2** (Figure 3). The shortest intermolecular Cl···Cl distance is *ca.* 4.073 Å [Cl1···Cl3d; (d) = x-1, y, z], whereas the shortest Ru···Ru separation is approximately 6.996 Å [Ru(1)···Ru(1e); (e) = x, -y+1, z-1/2]. Finally, π···Cl contacts, which cover the range *ca.* 3.18(1)-3.47(1) Å, stabilize the crystal structure of **2**.

Preprints (www.preprints.org) | NOT PEER-REVIEWED | Posted: 11 August 2022 doi:10.20944/preprints202208.0217.v1

2.2 Computed Hirshfeld Surfaces

Hirshfeld surfaces of the neutral [$RuCl_4$(Hgua)(dmso)] and [$RuCl_4$(Hgua)(gua)] complexes were obtained and their intermolecular contacts were studied by means of CrystalExplorer [16,17]. The surfaces were drawn considering the distances from a point on the surface to the nearest atom outside (d_e) and inside (d_i) their surfaces. Any restriction associated to the size of the involved atoms was corrected through a normalized distance, named d_{norm}, which was analyzed as previously done [18-20].

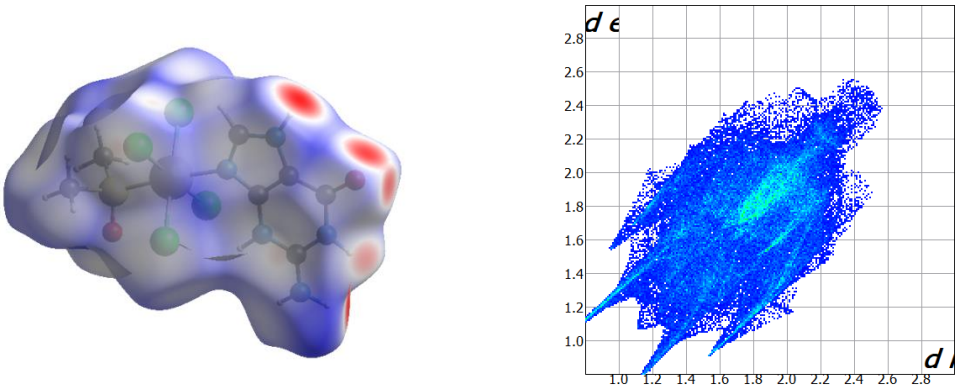

(**a**) (**b**)

Figure 4. (**a**) Hirshfeld surface of **1** calculated through d_{norm} function; (**b**) Fingerprint maps for compound **1** (see text).

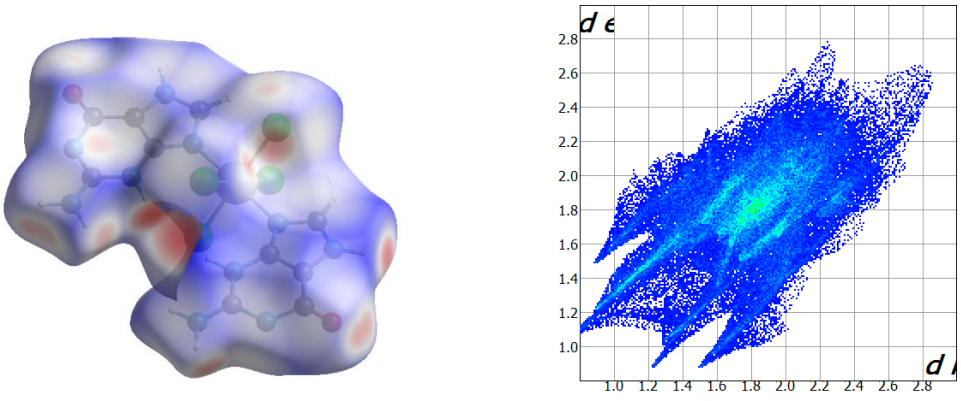

(**a**) (**b**)

Figure 5. (**a**) Hirshfeld surface of **2** calculated through d_{norm} function; (**b**) Fingerprint maps for compound **2** (see text).

The Hirshfeld surfaces, along with their fingerprint maps, for complexes **1** and **2** are given in Figures 4 and 5, respectively. Shorter contacts are displayed by using red color, whereas white color is assigned to interactions around the van der Waals distance [16,17]. In **1**, the most relevant contacts are H···O interactions involving water molecules and also interactions between carbonyl and amino groups of neighboring guanine molecules. These contacts gave *ca.* 26.4% of the fingerprint plot (Figure 4). Moreover, intermolecular Cl···H interactions, which are mainly generated by chloride ions and water molecules, cover approximately 21.8% of the full fingerprint plot of **1** (Figure 4). In compound **2**, the

Preprints (www.preprints.org) | NOT PEER-REVIEWED | Posted: 11 August 2022 doi:10.20944/preprints202208.0217.v1

Cl···H interactions, with a value of 17.5% of the full fingerprint plot, represent a percentage lower than that found in **1**, whereas the H-bonding H···O interactions cover pretty much the same value in both compounds, this value being approximately 26.5% of the complete fingerprint plot of **2** (Figure 5).

2.3 Magnetic properties

2.3.1 Dc magnetic susceptibility

The magnetic properties of **1** and **2** were investigated through direct current (dc) magnetic susceptibility measurements on polycrystalline samples in the range of temperature 300-2 K and along with an external dc magnetic field (H_{dc} = 0.5 T). $\chi_M T$ *versus* T plots for compounds **1** and **2** [χ_M being the molar magnetic susceptibility per Ru(III) ion] are given in Figure 6. At T = 300 K, $\chi_M T$ values are approximately 0.58 (**1**) and 0.54 $cm^3mol^{-1}K$ (**2**), which are very close to those earlier published for mononuclear Ru(III) compounds with low-spin configuration (t_{2g}^5) and S = 1/2 for this $4d^5$ metal ion [21–24]. Upon cooling, $\chi_M T$ for **1** decreases constantly to *ca*. 70 K and then more slowly with decreasing temperature, reaching a minimum value of 0.49 $cm^3mol^{-1}K$ at 30 K. Then, it increases gradually to a maximum value of *ca*. 0.66 $cm^3mol^{-1}K$ at 2.0 K (Figure 6). In contrast, $\chi_M T$ for **2** continuously decreases with decreasing temperature, showing a linear dependence and reaching a final value of approximately 0.46 $cm^3mol^{-1}K$ at 2.0 K (Figure 7). The decrease observed for the $\chi_M T$ value of both compounds at medium-high temperature would occur as a result of the spin–orbit coupling (SOC) of the $^2T_{2g}$ ground term and its orbital contribution [21,22]. The increase of the $\chi_M T$ value observed at low T values for **1** would indicate the phenomenon of an unprecedented intermolecular ferromagnetic exchange in a mononuclear Ru(III) complex. This magnetic behavior has been previously studied in complexes containing a magnetically-active 5d ion, but never before on a paramagnetic 4d metal ion [14,15].

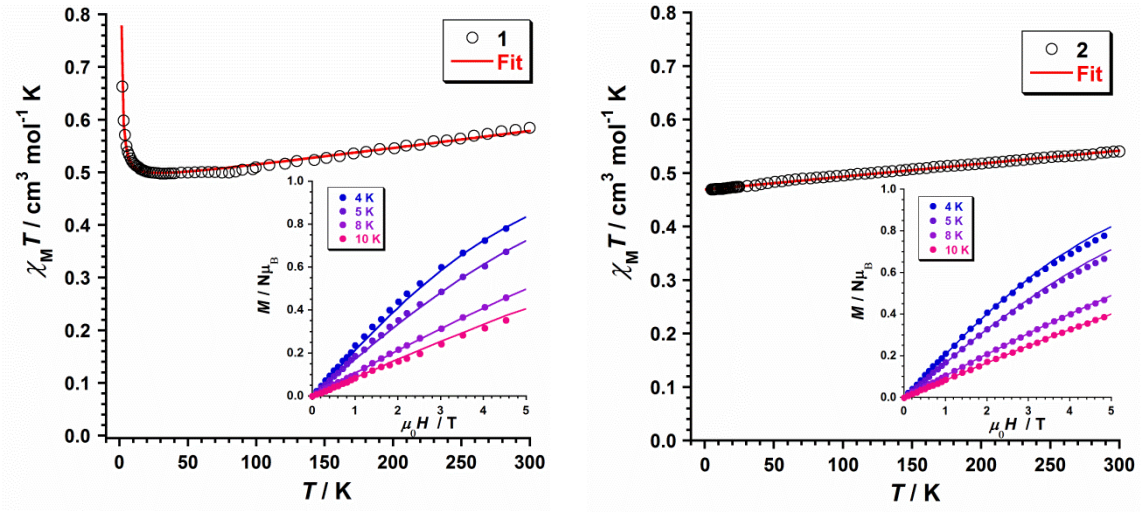

(**a**) (**b**)

Figure 6. (**a**) Plot of $\chi_M T$ vs. T obtained for compound **1**, the solid red line being the best fit. The inset displays the M *versus* H plot for **1**; (**b**) Plot of $\chi_M T$ vs. T obtained for compound **2**, the solid red line being the best fit. The inset displays the M *versus* H plot for **2**.

$$\hat{H} = -k\boldsymbol{L}\hat{S} + \Delta[\boldsymbol{L}_Z^2 - (1/3)\boldsymbol{L}(\boldsymbol{L}+1)] + \beta H(-k\boldsymbol{L} + 2\hat{S}) \quad (1)$$

To investigate the magnetic properties of **1** and **2**, the Hamiltonian of equation (1) and its theoretical expression for the magnetic susceptibility, adding a θ

Preprints (www.preprints.org) | NOT PEER-REVIEWED | Posted: 11 August 2022 doi:10.20944/preprints202208.0217.v1

parameter to explain any intermolecular interaction, was used as previously done for similar complexes with S = 1/2 [25,26]. Besides, the PHI program was employed for comparing the results of some of the fitted values [27]. The three sections in equation (1) can be assigned to the SOC, the field-ligand axial distortion and the Zeeman effect, respectively. It deserves to be mentioned that the three main parameters in equation (1) [considering $\boldsymbol{L}$ = 1, S = 1/2 and $g_{\parallel} = g_{\perp} = g$ for both **1** and **2**], namely, energy gap (Δ), orbital reduction factor (κ) and the spin-orbit coupling constant (λ), are strongly correlated [25,26]. The experimental data of the $\chi_M T$ *versus* T curves of **1** and **2** can be reproduced with the following parameters: Δ = 913 cm^{-1}, κ = 0.86, λ = -865 cm^{-1} and θ = +0.57 cm^{-1} for **1** and Δ = 1140 cm^{-1}, κ = 0.81 and λ = -885 cm^{-1} for **2**. Besides, the g and θ values were in good agreement with the simulation obtained through PHI program [g = 2.26, θ = +0.57 cm^{-1} and χ_{TIP} = 326 x 10^{-6} cm^3mol^{-1} for **1** and g = 2.23, and χ_{TIP} = 244 x 10^{-6} cm^3mol^{-1} for **2**] and were used to simultaneously fit the field dependence of the molar magnetization (M) plots at several temperatures for **1** and **2** [9], which are given in the respective insets of Figure 6. In general, the computed curves fit well the experimental data at the studied temperatures. The parameters thus obtained are very close to those of earlier published Ru(III) compounds [21–24]. The positive θ value obtained for **1** would indicate the presence of a ferromagnetic exchange coupling for this compound. It is well-known that short halogen···halogen intermolecular contacts can transmit antiferromagnetic couplings between neigboring paramagnetic metal ions [28-34], but ferromagnetic exchange couplings thus obtained are uncommon [14,15]. A suitable spatial arrangement of the mononuclear [$RuCl_4$(Hgua)(gua)] units with Ru–Cl···π···Cl–Ru interactions, as shown in Figure 2b, would generate a spin polarization by means of guanine rings between close [$RuCl_4$(Hgua)(gua)] units, and would explain the unprecedented ferromagnetic behavior observed only for **1**.

2.3.2 Ac magnetic susceptibility

Alternating current (ac) magnetic susceptibility studies on polycrystalline samples of **1** and **2** were carried out, and it was observed that none of them showed out-of-phase ac signals (χ''_M) at H_{dc} = 0 G. Nonetheless, compound **2** displays ac signals at low temperatures when an external dc magnetic field is utilized (H_{dc} = 2500 and 5000 G). In the case of compound **1**, structural factors and/or a strong quantum tunneling of the magnetization (QTM), would cancel any slow relaxation of the magnetization for this other mononuclear Ru(III) complex. The features observed for **2** are characteristic of compounds displaying slow relaxation of magnetization, what is called Single-Ion Magnet (SIM) behavior when they are mononuclear systems [19,35]. These out-of-phase ac signals obtained at 2500 and 5000 G are given as χ''_M *versus* ν plots in Figure 7. As one can observe, the number of χ''_M maxima, as well as their intensity, increase with increasing the utilized dc magnetic field. Besides, these χ''_M maxima shift to higher frequencies with increasing the external magnetic field (Figure 7).

Preprints (www.preprints.org) | NOT PEER-REVIEWED | Posted: 11 August 2022 doi:10.20944/preprints202208.0217.v1

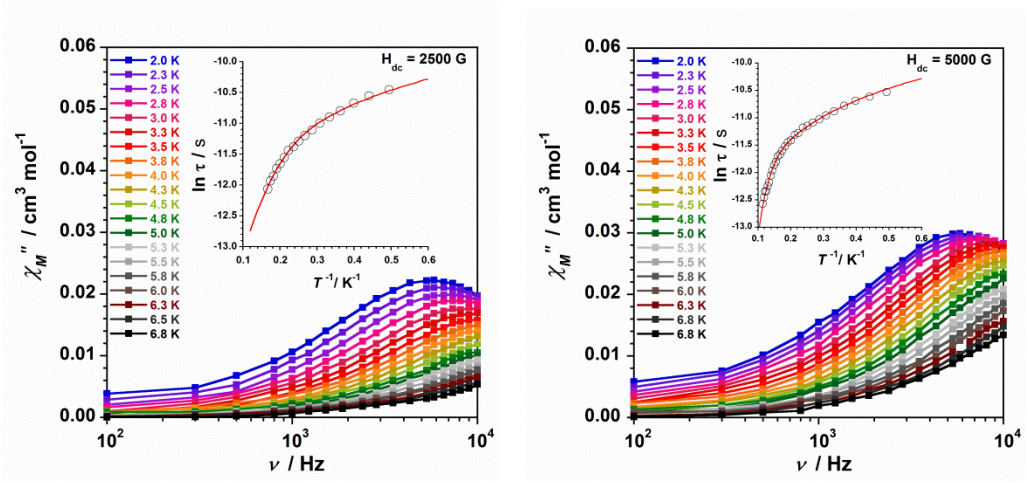

(**a**) (**b**)

Figure 7. (**a**) Out-of-phase ac susceptibility *versus* frequency plot under an external dc field of 2500 G for **1**. The inset is the ln(τ) *versus* 1/*T* plot with the fit considering the contribution of two relaxation mechanisms (Orbach + direct); (**b**) Out-of-phase ac susceptibility *versus* frequency plot under an external dc field of 5000 G for **2**. The inset is the ln(τ) *versus* 1/*T* plot with the fit considering the contribution of two relaxation mechanisms (Orbach + direct).

$$\tau^{-1} = \tau^{-1}_{\text{ORBACH}} + \tau^{-1}_{\text{DIRECT}} + \tau^{-1}_{\text{RAMAN}} + \tau^{-1}_{\text{QTM}} \quad (2)$$

Through the data of the out-of-phase ac susceptibility, the ln(τ) *versus* 1/*T* plots at 2500 and 5000 G were obtained for complex **2** (insets in Figure 7). These data draw curved lines which would account for the occurrence of at least two relaxation processes in compound **2**. As a result, the whole ln(τ) *versus* 1/*T* curve could be fitted through equation (2), where several mechanisms for spin-lattice relaxation of magnetization could be examined, that is, Orbach [$\tau_o^{-1}\exp(-U_{eff}/k_BT)$; with τ_o being the preexponential factor, τ is the relaxation time, U_{eff} is the anisotropy energy barrier to the magnetization reorientation, and k_B is the Boltzmann constant], direct (AT), Raman (CT^n), and Quantum Tunnelling (QTM). All these relaxation processes were analyzed during the fitting method of the ln(τ) *versus* 1/*T* curves for **2**, even though the best fit was that obtained when considering the Orbach and direct mechanisms. Thus, taking into account only Orbach and direct processes, the best least-squares fit of the experimental data of **2** gave as result: $\tau_o = 2.6 \times 10^{-7}$ s, $U_{eff} = 17.1$ cm^{-1} and $A = 17464$ s^{-1}K^{-1} for data obtained at 2500 G and $\tau_o = 1.7 \times 10^{-8}$ s, $U_{eff} = 36.6$ cm^{-1} and $A = 17454$ s^{-1}K^{-1} for data obtained at 5000 G. From these results, which are somewhat unsimilar to those of other SIMs of metal ions with S = 1/2 [36,37], it is worthy to point out that the energy barrier value (U_{eff}) increases with increasing field, the external dc magnetic field of 5000 G being optimal for **2**. Indeed, the values of the U_{eff} parameter computed for **2** are higher than that reported for the first Ru(III)-based SIM, the $[RuCl_3(PPh_3)_2(MeCN)]$ complex, with $\tau_o = 9.8 \times 10^{-6}$ s and $U_{eff} = 15.3$ cm^{-1}, these values being obtained through the Arrhenius equation [9]. Nevertheless, for this other Ru(III)-based SIM, it was suggested a phonon-bottlenecked direct relaxation for temperatures up to 10 K [9].

In any case, this comparison shows that both Ru(III) SIMs display relaxation dynamics with distinct relaxation pathways and further detailed magnetic and theoretical studies performed on different Ru(III) complexes will be necessary to correctly understand the relaxation dynamics of Ru(III)-based SIMs.

Preprints (www.preprints.org) | NOT PEER-REVIEWED | Posted: 11 August 2022 doi:10.20944/preprints202208.0217.v1

3. Materials and Methods

3.1. Reagents and Instruments

All the synthesis were carried out under aerobic conditions, by using reagents as received. The ruthenium precursor $(PPh_4)_2[\{RuCl_4(H_2O)\}_2(\mu\text{-}O)]\cdot 4H_2O$ was obtained following the synthetic method previously described in the literature [18]. SEM-EDX analyses were obtained through a Hitachi S-4800 field emission scanning electron microscope, and elemental analyses (C, H, N) were performed by the Central Service for the Support to Experimental Research (SCSIE) at the University of Valencia. Infrared spectra of **1** and **2** were recorded with a PerkinElmer Spectrum 65 FT-IR spectrometer (4000-400 cm^{-1} region). Variable-temperature, solid-state (dc and ac) magnetic susceptibility data down to 2.0 K were collected on a Quantum Design MPMS-XL SQUID magnetometer equipped with a 5 T dc magnet. Experimental magnetic data were corrected for the diamagnetic contributions of the involved atoms by using Pascal's constants [38].

3.2. Preparation of the Compounds

3.2.1. Synthesis of $[RuCl_4(Hgua)(dmso)]\cdot 2H_2O$ (**1**)

Guanine (0.06g, 0.40 mmol) was dissolved in a dmso:HCl mixture (20 mL, 1.0 M, 5:1, v/v) and added drop by drop to a refluxing solution of $(PPh_4)_2[\{RuCl_4(H_2O)\}_2(\mu\text{-}O)]\cdot 4H_2O$ (0.198 g, 0.15 mmol) in dmso (30 mL). Then, the reflux was kept for 24 h. The resulting reddish-brown solution was filtered and then heated at 60 °C until the solvent was left to evaporate. The solid residue was collected with HCl (10 mL, 1.0 M) and the generated solution was filtered. EtOH (10 mL) was poured to the final solution that was left to evaporate at room temperature. Red crystals of **1** were obtained in 2 weeks. Yield: *ca.* 45%. Anal. Calcd. for $C_7H_{16}Cl_4N_5O_4SRu$ (**1**): C, 16.5; H, 3.2; N, 13.8%. Found: C, 16.7; H, 3.4; N, 13.7%. SEM-EDX analysis gave 1:1 (Ru/S) and 1:4 (Ru/Cl) molar ratios for **1**. IR (KBr pellets/cm^{-1}): the absorption associated to H_2O molecule occurs at 3423br and bands assigned to the coordinated/protonated guanine and dmso appear at 3240(m), 3194(s), 3117(w), 3005(w), 1718(s), 1669(vs), 1635(m), 1578(m), 1457(m), 1457(m), 1406(m), 1385(m), 1158(m), 1099(s), 765(m), 667(m), 545(m), and 497(m).

3.2.1. Synthesis of $[RuCl_4(Hgua)(gua)]\cdot 3H_2O$ (**2**)

$K_2[RuCl_5(H_2O)]$ (11.2 mg, 0.03 mmol) and guanine (6.80 mg, 0.03 mmol) were reacted by means of a solvothermal synthesis in HCl (2.5 mL, 6.0 M) at 90 °C for two days, then a 48 h cooling process took place to room temperature. Orange cubes of **2** were thus obtained. Yield: *ca.* 35%. Anal. Calcd. for $C_{10}H_{17}Cl_4N_{10}O_5Ru$ (**2**): C, 20.0; H, 2.9; N, 23.3%. Found: C, 20.3; H, 2.9; N, 23.6%. SEM-EDX analysis gave a 1:4 (Ru/Cl) molar ratio for **2**. IR peaks (KBr pellets, ν/cm^{-1}): 3402(m), 3330(sh), 3220(m), 3123(m), 2568(w), 2924(w), 1732(s), 1669(vs), 1635(s), 1559(m), 1473(m), 1456(m), 1370(m), 1300(w), 1258(w), 1204(m), 1149(s), 1052(m), 976(m), 760(s), 709(m), and 668(m).

3.3. X-ray data collection and structure refinement

X-ray diffraction data from a single crystal of dimensions 0.13 x 0.10 x 0.09 mm^3 (**2**) were collected on a Bruker D8 Venture diffractometer with graphite-monochromated Mo-K_α radiation (λ = 0.71073 Å). The resulting crystal and refinement parameters for **1** and **2** are given in Table 1. The structure of **2** was solved by standard direct methods and in turn completed by Fourier recycling by using the SHELXTL software packages. The model thus obtained was refined through version 2018/1 of SHELXL against F^2 on all data by full-matrix least squares [39]. All non-hydrogen atoms were refined anisotropically. The hydrogen atoms of the guanine molecules were set in calculated positions and refined isotropically by using the riding model. The H atoms of the disordered H_2O molecules in **2**

 doi:10.20944/preprints202208.0217.v1

were neither detected nor included in the model. Graphical manipulations were carried out through DIAMOND [40]. CCDC code for **2**: 2191993.

4. Conclusions

In summary, we have characterized magnetostructurally two novel mononuclear guanine-based Ru(III) compounds of formula *trans*-[$RuCl_4$(Hgua)(dmso)]·$2H_2O$ (**1**) and *trans*-[$RuCl_4$(Hgua)(gua)]·$3H_2O$ (**2**) [Hgua = protonated guanine (gua), dmso = dimethyl sulfoxide]. The two Ru^{III} complexes are self-assembled through an extended network of N-H···Cl hydrogen bonds and π···Cl intermolecular contacts, which generates novel supramolecular structures based on this 4d metal ion. The investigation of the magnetic properties of **1** and **2** by means of dc magnetic susceptibility data reveals a different magnetic behavior. While **1** is a ferromagnetic compound at low temperatures, **2** exhibits a behavior characteristic of magnetically isolated mononuclear Ru(III) complexes with S = 1/2. In addition, the ac magnetic susceptibility experimental data reveal slow relaxation of the magnetization in the presence of external dc fields only for **2**, hence indicating the occurrence of field-induced single-ion magnet (SIM) behavior in this mononuclear guanine-based Ru(III) complex. In fact, the U_{eff} value for **1** is higher than that of an earlier published Ru(III)-based SIM. Anyway, more theoretical and experimental studies will need to fully understand the relaxation dynamics of the very interesting Ru(III)-based SIMs.

Supplementary Materials: The following supporting information can be downloaded at: www.mdpi.com/xxx/s1. X-ray crystallographic data in CIF format for compound **2**.

Author Contributions: Conceptualization, F.L. and J.M.L.; funding acquisition, F.L. and J.M.L.; methodology, M.O.A; N.M. and J.M.L.; investigation, M.O.A; N.M.; F.L. and J.M.L.; formal analysis, M.O.A; N.M. and J.M.L.; writing—original draft preparation, J.M.L.; writing—review and editing, J.M.L. All authors have read and agreed to the published version of the manuscript.

Funding: This research was funded by the VLC-BIOCLINIC Program of the University of Valencia [Project PI-2021-007-DIRUGEN] and the Spanish Ministry of Science and Innovation [Projects PID2019-109735GB-I00 and CEX2019-000919-M (Excellence Unit "María de Maeztu")].

Institutional Review Board Statement: Not applicable.

Informed Consent Statement: Not applicable.

Data Availability Statement: The raw data that support the findings of this study are available from the corresponding author upon reasonable request.

Acknowledgments: M.O.A. thanks the Spanish "FPI fellowships" Program.

Conflicts of Interest: The authors declare no conflict of interest.

References

1. Li, F.; Collins, J.G.; Keene, F.R. Ruthenium complexes as antimicrobial agents. *Chem. Soc. Rev*. **2015**, *44*, 2529-2542.
2. Hartinger, C.G.; Zorbas-Seifried, S.; Jakupec, M.A.; Kynast, ,B.; Zorbas, H.; Keppler, B.K. From bench to bedside-preclinical and early clinical development of the anticancer agent indazolium trans-[tetrachlorobis(1H-indazole)ruthenate(III)] (KP1019 or FFC14A). *J. Inorg. Biochem*. **2006**, *100*, 891-904.
3. Hartinger, C.G.; Jakupec, M.A.; Zorbas-Seifried, S.; Groessl, M.; Egger, A.; Berger, W.; Zorbas, H.; Dyson, P.J.; Keppler, B.K. KP1019, A New Redox-Active Anticancer Agent – Preclinical Development and Results of a Clinical Phase I Study in Tumor Patients. *Chem. Biodivers*. **2008**, *5*, 2140-2155.
4. Ang, W.H.; Casini, A.; Sava, G.; Dyson, P.J. Organometallic ruthenium-based antitumor compounds with novel modes of action. *J. Organomet. Chem*. **2011**, *696*, 989-998.
5. Turel, I; Pečanac, M.; Golobič, A.; Alessio, E.; Serli, B.; Bergamo, A.; Sava, G. Solution, solid state and biological characterization of ruthenium(III)-DMSO complexes with purine base derivatives. *J. Inorg. Biochem*. **2004**, *98*, 393-401.
6. Correa, R.S.; Freire, V.; Barbosa, M.I.F.; Bezerra, D.P.; Bomfim, L.M.; Moreira, D.R.M.; Soares, M.B.P.; Ellena, J.; Batista, A.A. Ru(II)–thyminate complexes: New metallodrug candidates against tumor cells. *New J. Chem*. **2018**, *42*, 6794-6802.
7. Silva, S.L.R.; Baliza, I.R.S.; Dias, R.B.; Sales, C.B.S.; Rocha, C.A.G.; Soares, M.B.P.; Correa, R.S.; Batista, A.A.; Bezerra, D.P. Ru(II)-thymine complex causes DNA damage and apoptotic cell death in human colon carcinoma HCT116 cells mediated by JNK/p38/ERK1/2 via a p53-independent signaling. *Sci. Rep*. **2019**, *9*, 11094.
8. Orts-Arroyo, M.; Gutiérrez, F.; Gil-Tebar, A.; Ibarrola-Villava, M.; Jiménez-Martí, E.; Silvestre-Llora, A.; Castro, I.; Ribas, G.; Martínez-Lillo, J. A novel adenine-based diruthenium(III) complex: Synthesis, crystal structure, electrochemical properties and evaluation of the anticancer activity. *J. Inorg. Biochem*. **2022**, *232*, 111812.
9. Wu, S.-Q.; Miyazaki, Y.; Nakano, M.; Su, S.-Q.; Yao, Z.S.; Kou, H.-Z.; Sato, O. Slow Magnetic Relaxation in a Mononuclear Ruthenium(III) Complex. *Chem. Eur. J*. **2017**, *23*, 10028-10033.
10. Colacio, E; Crespo, O.; Cuesta, R.; Kivekas, R.; Laguna, A. [Au_2(μ-G)(μ-dmpe)]·$(KBr)_{0.75}$·$2H_2O$, a cyclic dinuclear gold(I) complex with an N3,N9-bridging coordination mode of guanine and aurophilic interactions: synthesis, X-ray crystal structure and luminescence properties (dmpe=1,2-bis(dimethylphosphino)ethane and G=guaninato dianion). *J. Inorg. Biochem*. **2004**, *98*, 595-600.
11. Gaballa, A.S.; Schmidt, H., Wagner, Ch.; Steinborn, D. Structure and characterization of platinum(II) and platinum(IV) complexes with protonated nucleobase ligands. *Inorg. Chim. Acta* **2008**, *361*, 2070-2080.
12. Gupta, D.; Nowak, R.; Lippert, B. Pt(II) complexes of unsubstituted guanine and 7-methylguanine. *Dalton Trans*. **2010**, *39*, 73-84.
13. Orts-Arroyo, M.; Silvestre-Llora, A.; Castro, I.; Martínez-Lillo, J. Molecular Self-Assembly of an Unusual Dinuclear Ruthenium(III) Complex Based on the Nucleobase Guanine. *Crystals* **2022**, *12*, 448.
14. Martínez-Lillo, J.; Armentano, D.; De Munno, G.; Marino, N.; Lloret, F.; Julve, M.; Faus, J. A self-assembled tetrameric water cluster stabilized by the hexachlororhenate(IV) anion and diprotonated 2,2′-biimidazole: X-ray structure and magnetic properties. *CrystEngComm* **2008**, *10*, 1284-1287.
15. Martínez-Lillo, J.; Pedersen, A.H.; Faus, J.; Julve, M.; Brechin, E.K. Effect of Protonated Organic Cations and Anion−π Interactions on the Magnetic Behavior of Hexabromorhenate(IV) Salts. *Cryst. Growth Des*. **2015**, *15*, 2598-2601.
16. Spackman, M.A.; Jayatilaka, D. Hirshfeld surface analysis. *CrystEngComm* **2009**, *11*, 19-32.
17. Turner, M.J.; McKinnon, J.J.; Wolff, S.K.; Grimwood, D.J.; Spackman, P.R.; Jayatilaka, D.; Spackman, M.A. Crystal Explorer 17; University of Western Australia: Perth, Australia, 2017.
18. Orts-Arroyo, M.; Castro, I.; Lloret, F.; Martínez-Lillo, J. Molecular Self-Assembly in a Family of Oxo-Bridged Dinuclear Ruthenium(IV) Systems. *Cryst. Growth Des*. **2020**, *20*, 2044-2056.
19. Sanchis-Perucho, A.; Orts-Arroyo, M.; Camús-Hernández, J.; Rojas-Dotti, C.; Escrivà, E.; Lloret, F.; Martínez-Lillo, J. Hexahalorhenate(IV) salts of protonated ciprofloxacin: Antibiotic-based single-ion magnets. *CrystEngComm* **2021**, 23, 8579-8587.
20. Orts-Arroyo, M.; Ten-Esteve, A.; Ginés-Cárdenas, S.; Castro, I.; Martí-Bonmatí, L.; Martínez-Lillo, J. A gadolinium(III) complex based on the thymine nucleobase with properties suitable for magnetic resonance imaging. *Int. J. Mol. Sci*. **2021**, 22, 4586.
21. Yeung, W.F.; Man, W.-L.; Wong, W.-T.; Lau, T.-C.; Gao, S. Ferromagnetic Ordering in a Diamond-Like Cyano-Bridged $Mn^{II}Ru^{III}$ Bimetallic Coordination Polymer. *Angew. Chem. Int. Ed.* **2001**, *40*, 3031-3033.
22. Toma, L.M.; Toma, L.D.; Delgado, F.S.; Ruiz-Pérez, C.; Sletten, J.; Cano, J.; Clemente-Juan, J.M.; Lloret, F.; Julve, M. Trans-dicyanobis(acetylacetonato)ruthenate(III) as a precursor to build novel cyanide-bridged Ru^{III}–M^{II} bimetallic compounds [M = Co and Ni]. *Coord. Chem. Rev*. **2006**, *250*, 2176-2193.
23. Armentano, D.; Martínez-Lillo, J. Hexachlororhenate(IV) salts of ruthenium(III) cations: X-ray structure and magnetic properties. *Inorg. Chim. Acta* **2012**, *380*, 118-124.
24. Palacios, M.A.; Mota, A.J.; Ruiz, J., Hänninen, M.M.; Sillanpää, R.; Colacio, E. Diphenoxo-Bridged $Ni^{II}Ln^{III}$ Dinuclear Complexes as Platforms for Heterotrimetallic $(Ln^{III}Ni^{II})_2Ru^{III}$ Systems with a High-Magnetic-Moment Ground State: Synthesis, Structure, and Magnetic Properties. *Inorg. Chem*. **2012**, *51*, 7010-7012.
25. Pacheco, M.; Cuevas, A.; González-Platas, J.; Faccio, R.; Lloret, F.; Julve, M.; Kremer, C. Synthesis, crystal structure and magnetic properties of the Re(II) complexes NBu_4[Re(NO)Br_4(L)] (L = pyridine and diazine type ligands). *Dalton Trans*. **2013**, *42*, 15361-15371.
26. Pacheco, M.; Cuevas, A.; González-Platas, J.; Lloret, F.; Julve, M.; Kremer, C. The crystal structure and magnetic properties of 3-pyridinecarboxylate-bridged Re(II)M(II) complexes (M = Cu, Ni, Co and Mn). *Dalton Trans*. **2015**, *44*, 11636-11648.

27. Chilton, N.F.; Anderson, R.P.; Turner, L.D.; Soncini, A.; Murray, K.S. PHI: A powerful new program for the analysis of anisotropic monomeric and exchange-coupled polynuclear d- and f-block complexes. *J. Comput. Chem*. **2013**, *34*, 1164-1175.
28. González, R.; Chiozzone, R.; Kremer, C.; Guerra, F.; De Munno, G.; Lloret, F.; Julve, M.; Faus, J. Magnetic Studies on Hexaiodorhenate(IV) Salts of Univalent Cations. Spin Canting and Magnetic Ordering in $K_2[ReI_6]$ with Tc = 24 K. *Inorg. Chem*. **2004**, *43*, 3013-3019.
29. Martínez-Lillo, J.; Armentano, D.; De Munno, G.; Lloret, F.; Julve, M.; Faus, J. A Two-Dimensional $Re^{IV}Ag^{I}$ Compound: X-ray Structure and Magnetic Properties. *Cryst. Growth Des*. **2006**, *6*, 2204-2206.
30. Martínez-Lillo, J.; Armentano, D.; De Munno, G.; Faus, J. Magneto-structural study on a series of rhenium(IV) complexes containing biimH_2, pyim and bipy ligands. *Polyhedron* **2008**, *27*, 1447-1454.
31. Martínez-Lillo, J.; Faus, J.; Lloret, F.; Julve, M. Towards multifunctional magnetic systems through molecular-programmed self assembly of Re(IV) metalloligands. *Coord. Chem. Rev*. **2015**, *289-290*, 215-237.
32. Martínez-Lillo, J.; Kong, J.; Julve, M.; Brechin, E.K. Self-Assembly of the Hexabromorhenate(IV) Anion with Protonated Benzotriazoles: X-ray Structure and Magnetic Properties. *Cryst. Growth Des*. **2014**, *14*, 5985-5990.
33. Armentano, D; Barquero, M.A.; Rojas-Dotti, C.; Moliner, N.; De Munno, G.; Brechin, E.K.; Martínez-Lillo, J. Enhancement of Intermolecular Magnetic Exchange through Halogen···Halogen Interactions in Bisadeninium Rhenium(IV) Salts. *Cryst. Growth Des*. **2017**, 17, 5342-5348.
34. Armentano, D.; Sanchis-Perucho, A.; Rojas-Dotti, C.; Martínez-Lillo, J. Halogen···halogen interactions in the self-assembly of one-dimensional 2,2′-bipyrimidine-based $Cu^{II}Re^{IV}$ systems. *CrystEngComm*, **2018**, *20*, 4575-4581.
35. Rojas-Dotti, C; Sanchis-Perucho, A.; Orts-Arroyo, M.; Moliner, N.; González, R.; Lloret, F.; Martínez-Lillo, J. Field-Induced Single-Ion Magnet Phenomenon in Hexabromo- and Hexaiodorhenate(IV) Complexes. *Magnetochemistry* **2020**, *6*, 20.
36. Sanchis-Perucho, A.; J. Martínez-Lillo, J. Ferromagnetic exchange interaction in a new Ir(IV)–Cu(II) chain based on the hexachloroiridate(IV) anion. *Dalton Trans*. **2019**, *48*, 13925-13930.
37. Sanchis-Perucho, A.; J. Martínez-Lillo, J. A new family of one-dimensional bromo-bridged Ir(IV)–Cu(II) complexes based on the hexabromoiridate(IV) metalloligand. *Dalton Trans*. **2022**, *51*, 3323-3330.
38. Bain, G.A.; Berry, J.F. Diamagnetic Corrections and Pascal's Constants. *J. Chem. Educ*. **2008**, *85*, 532-536.
39. SHELXTL-2018/1, Bruker Analytical X-ray Instruments; Bruker: Madison, WI, USA, 2018.
40. DIAMOND 4.5.0, Crystal Impact GbR.; Crystal Impact: Bonn, Germany, 2018.